Physical Conditions in Shocked Interstellar Gas Interacting with the Supernova Remnant IC 443

Adam M. Ritchey[1], Edward B. Jenkins[2], Steven R. Federman[3], Johnathan S. Rice[3], Damiano Caprioli[4], and George Wallerstein[1]

[1]University of Washington [2]Princeton University [3]University of Toledo [4]University of Chicago

Abstract: We present the results of a detailed investigation into the physical conditions in interstellar material interacting with the supernova remnant IC 443. Our analysis is based on an examination of high-resolution *HST*/STIS and HET/HRS spectra of two stars probing predominantly neutral gas located both ahead of and behind the supernova shock front. The pre-shock neutral gas is characterized by densities and temperatures typical of diffuse interstellar clouds, while the post-shock material exhibits a range of more extreme physical conditions, including high temperatures (T > 10^4 K) in some cases, which may require a sudden heating event to explain. The ionization level is enhanced in the high-temperature post-shock material, which could be the result of enhanced radiation from shocks or from an increase in cosmic-ray ionization. The gas-phase abundances of refractory elements are also enhanced in the high-pressure gas, suggesting efficient destruction of dust grains by shock sputtering. Observations of highly-ionized species at very high velocity indicate a post-shock temperature of $T_s \approx 10^7$ K for the hot X-ray emitting plasma of the remnant's interior, in agreement with studies of thermal X-ray emission from IC 443.

HST and Ground-Based Observations:

High-resolution *HST*/STIS spectra were obtained for two stars probing IC 443: HD 43582, which probes the interior region of the supernova remnant, and HD 254755, which lies just beyond the bright optical filaments in the northeast (see Figure 1). This arrangement allows us to evaluate the physical conditions in interstellar material positioned both ahead of and behind the supernova shock front. The *HST* spectra have a velocity resolution of 2.8 km s^{-1} and cover the region from 1200 Å to 1397 Å. We also examine high S/N ratio ground-based spectra of our targets obtained using the High Resolution Spectrograph (HRS) of the 9.2 m Hobby Eberly Telescope (HET) at McDonald Observatory. The HET data have a velocity resolution of 3.1 km s^{-1} and cover much of the visible spectrum at high S/N (see Taylor et al. 2012).

Figure 2 presents the absorption profiles derived from our *HST* and HET observations of HD 254755 and HD 43582 for a selection of neutral and singly-ionized atomic species. Note the strong absorption from collisionally-excited fine-structure levels in the O I and Si II lines toward HD 43582. The O I* and O I** lines exhibit numerous distinct components between −50 and +50 km s^{-1}, while the Si II* and Ca II lines show additional components at velocities ranging from −100 to +100 km s^{-1}. The interstellar lines toward HD 254755 exhibit more moderate velocities, although the Ca II profile shows a high velocity component near −60 km s^{-1}.

Figure 3 presents the absorption profiles of the highly-ionized species Si III, Si IV, and N V, which are observed toward HD 43582. Most notable is the broad absorption feature detected in the high ions near −620 km s^{-1}, which likely probes rapidly expanding, shock-heated gas in the supernova remnant.

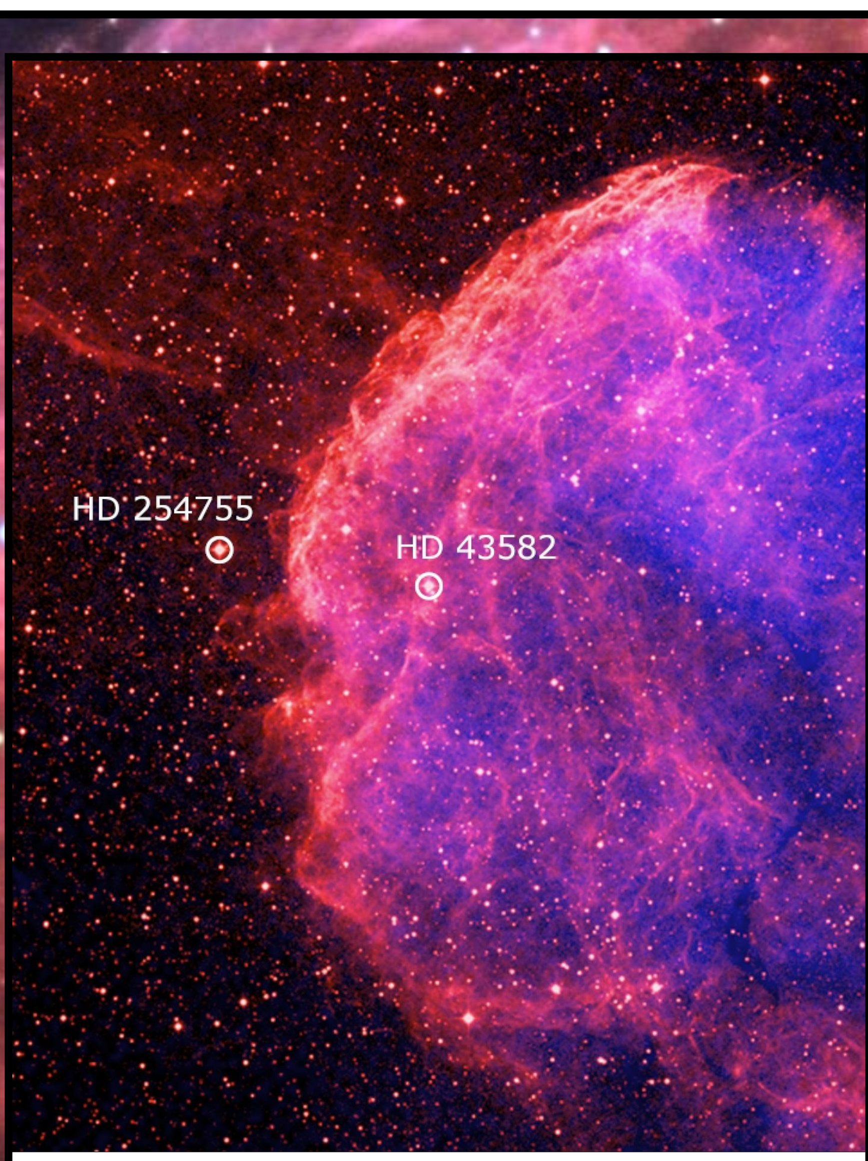

Figure 1: Composite image of IC 443. The optical image from the Digitized Sky Survey (red) is shown along with X-ray data (blue) from the *Chandra X-Ray Observatory* (Gaensler et al. 2006) and *ROSAT* (Asaoka & Aschenbach 1994). The stars targeted for *HST* observations are labeled.

Neutral and Singly-Ionized Atomic Species:

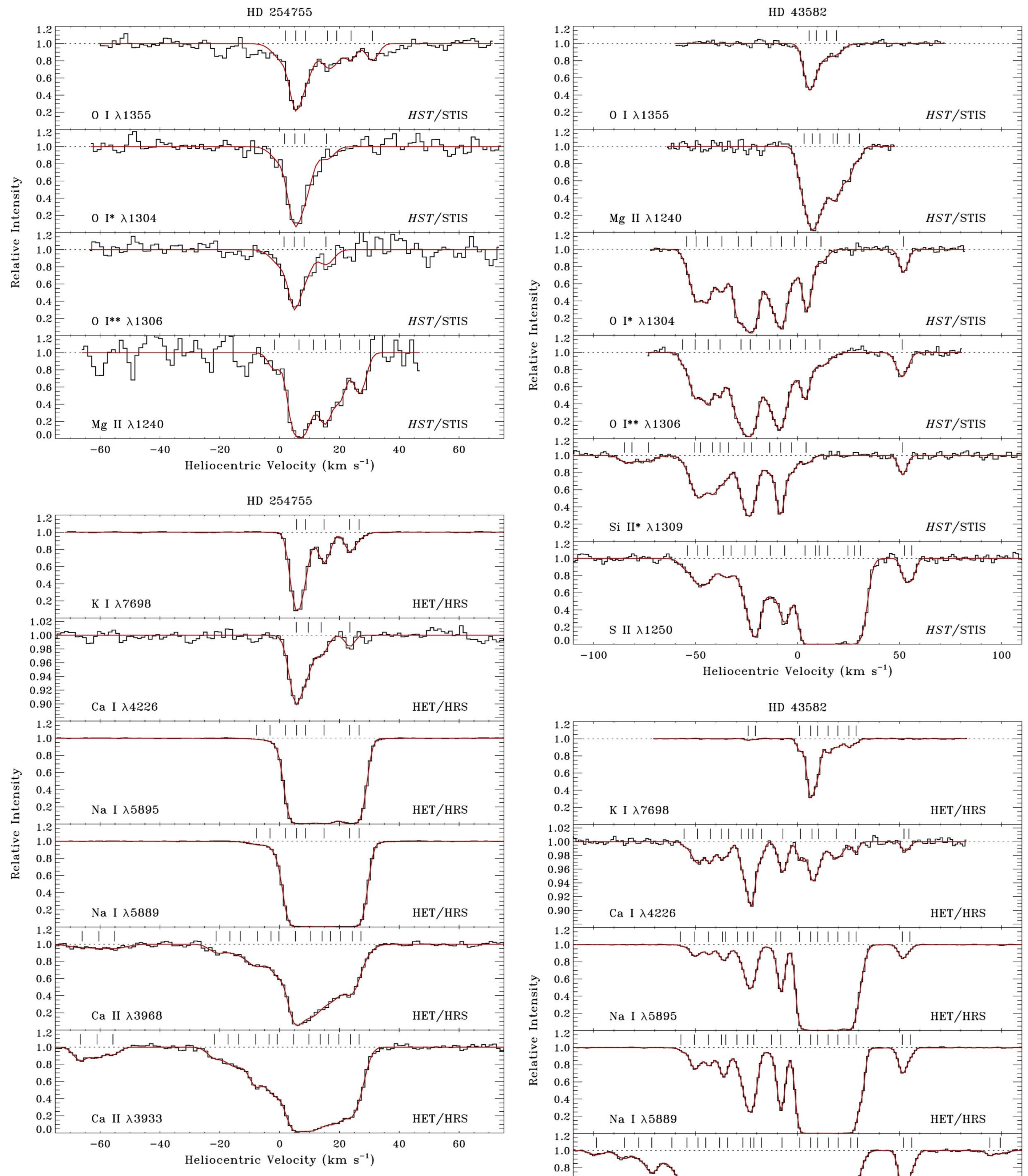

Figure 2: Interstellar absorption profiles of neutral and singly-ionized atomic species toward HD 254755 (left) and HD 43582 (right) from *HST*/STIS and HET/HRS data. The smooth red curves represent multi-component profile synthesis fits to the observed spectra shown as histograms. Tick marks indicate the positions of the velocity components included in the fits.

O I and Si II Excitations:

The relative populations of the O I and Si II fine-structure levels are sensitive probes of gas densities and kinetic temperatures. We use a combination of the N(O I*)/N(O I**) and [N(O I*) + N(O I**)]/N(O$_{\rm tot}$) ratios and the N(Si II*)/N(Si II) ratio to derive the total hydrogen density, n(H$_{\rm tot}$), kinetic temperature, T, and electron fraction, $x(e)$ = $n(e)/n$(H$_{\rm tot}$), as a function of velocity for the lines of sight to HD 43582 and HD 254755 (Figures 4 and 5).

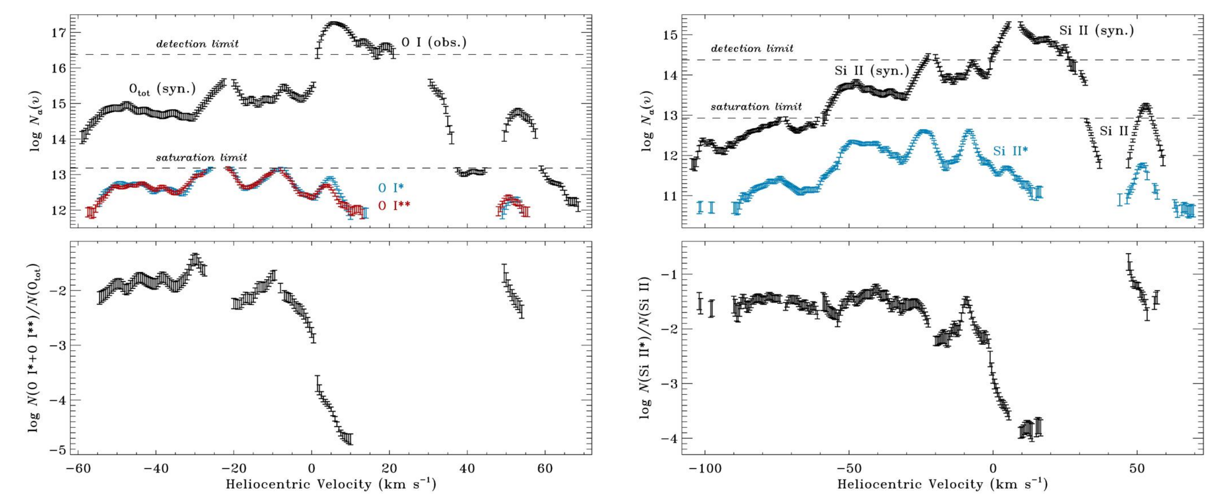

Figure 4: Upper panels: Apparent column density profiles of O I, O I*, and O I** (left) and Si II and Si II* (right) toward HD 43582. The O I λ1355 and Mg II λ1240 lines are used to define the O I and Si II profiles at the highest column densities. At more intermediate values, synthetic profiles are calculated using the S II λ1250 and λ1259 lines. Lower panels: The corresponding O I and Si II excitation ratios as a function of velocity.

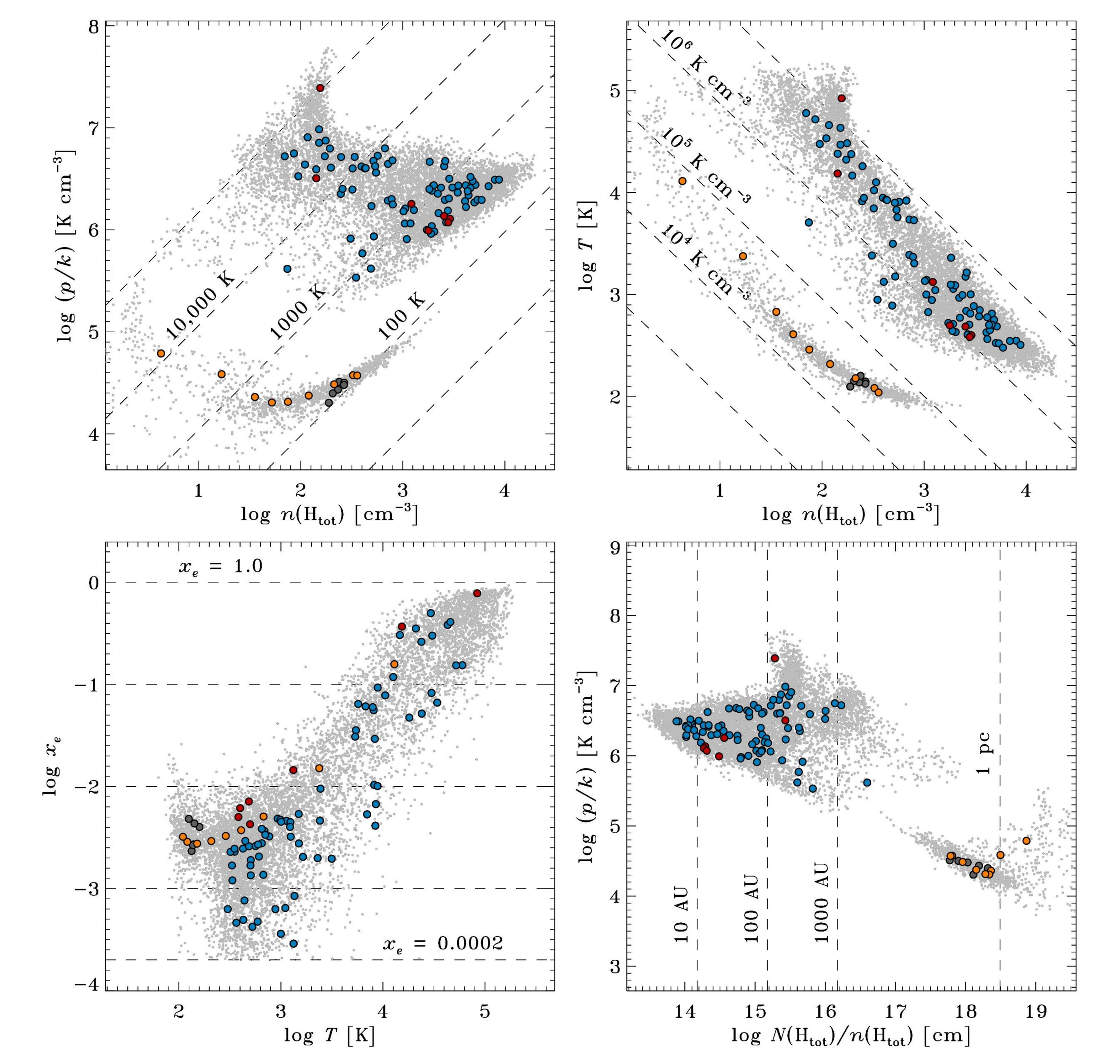

Figure 5: Pairwise plots of the physical conditions derived from our analysis of O I and Si II excitations for discrete velocity channels toward HD 43582 and HD 254755. Blue, orange, and red points denote high negative velocity gas, low velocity gas, and high positive velocity gas toward HD 43582. Dark gray points represent low velocity gas toward HD 254755. The underlying distribution of light gray points gives the range of physical conditions obtained when the input ratios are varied according to their 1σ uncertainties.

C I Excitations:

We disentangle the overlapping absorptions from the many C I multiplets covered by our *HST* observations using the methodology of Jenkins & Tripp (2001, 2011). The resulting apparent column density profiles of C I, C I*, and C I** toward HD 43582 are shown in Figure 6. These are used to produce the plot shown in Figure 7 of $f1$ = N(C I*)/N(C I$_{\rm tot}$) versus $f2$ = N(C I**)/N(C I$_{\rm tot}$), which allows us to estimate the thermal pressure in the gas as a function of velocity.

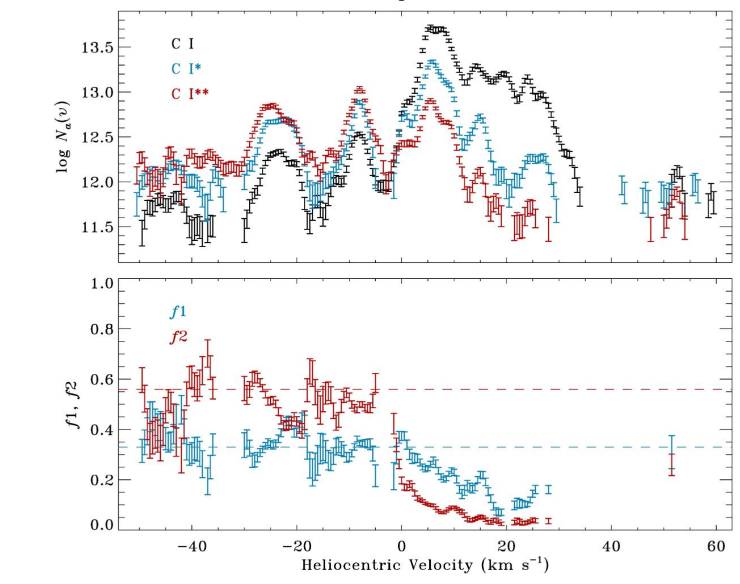

Figure 6: Upper panel: Apparent column density profiles of C I, C I*, and C I** toward HD 43582. Lower panel: The corresponding C I population ratios $f1$ and $f2$ plotted as a function of velocity.

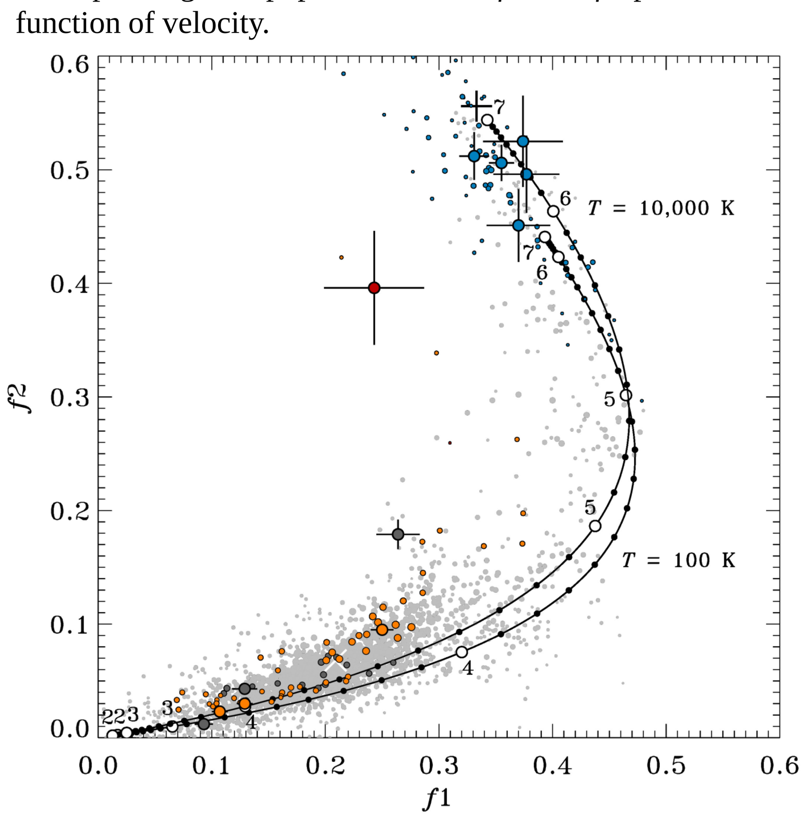

Figure 7: Relative C I fine-structure populations for velocity components toward HD 43582 and HD 254755. Large points with error bars show the outcomes from profile synthesis fits, while the smaller colored points correspond to the apparent column density measurements from Figure 6. The distribution of light gray points represents the outcomes obtained by Jenkins & Tripp (2011) for sight lines probing the local Galactic ISM. The curves represent theoretical expectations for two temperatures (as indicated) and for pressures in the range log (p/k) = 2 to 7.

Highly-Ionized Species:

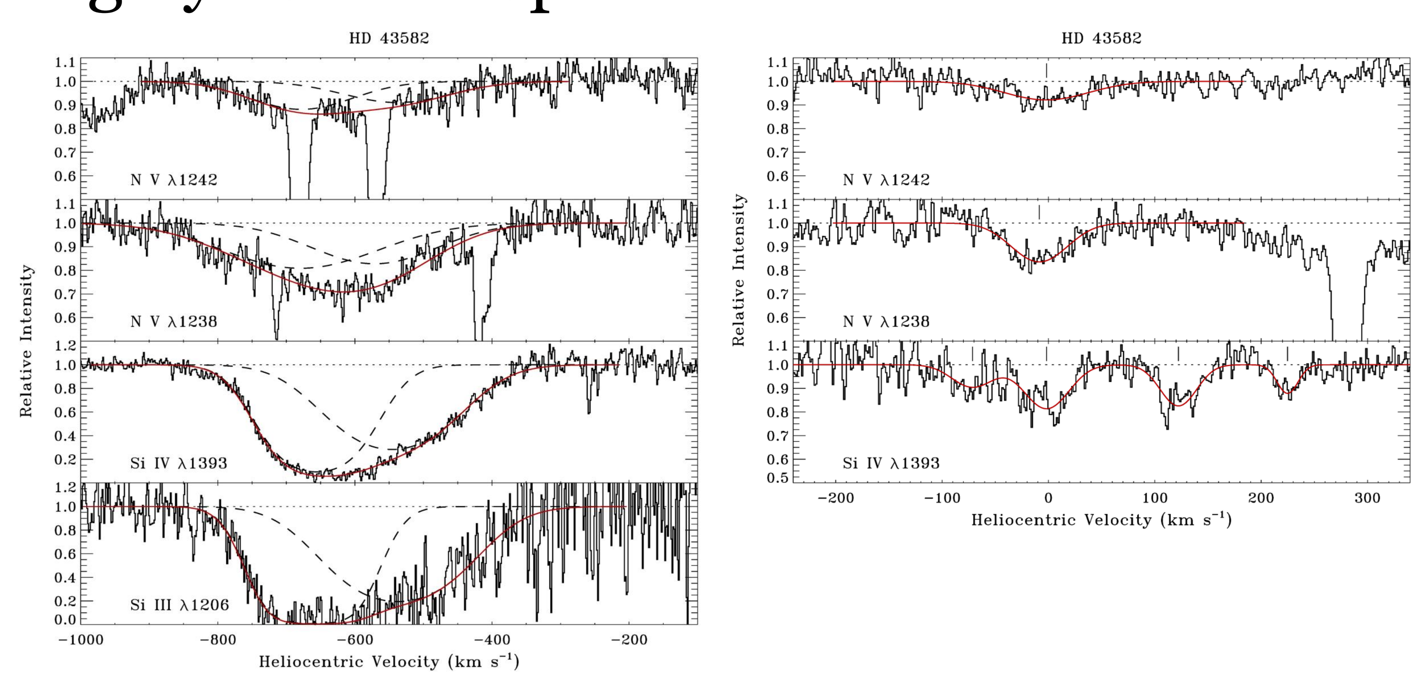

Figure 3: Absorption profiles of highly-ionized species observed toward HD 43582. The left panels present the Si III, Si IV, and N V profiles of a broad absorption feature detected near −620 km s^{-1}. The smooth red curves represent Voigt profile fits with dashed lines showing the contributions from two individual components. The right panels present the Si IV and N V profiles of the absorption features detected at more moderate velocities. (Absorption from Si III is probably also detected at these velocities. However, the flux is greatly depressed in this region by the nearby H I Lyα feature.) Tick marks indicate the positions of the components included in the fits. The Doppler parameters (b-values) imply temperatures of $T \approx 1.4 \times 10^7$ K for the two components that make up the broad absorption feature near −620 km s^{-1} and $T \approx 1.1 \times 10^6$ K for the narrower components observed at more moderate velocity.

Grain Destruction by Shocks:

The gas-phase abundances of the refractory elements Ni and Ca are enhanced in the high pressure gas seen mainly at negative velocities toward HD 43582 (Figure 8), an indication of efficient dust grain destruction by shock sputtering.

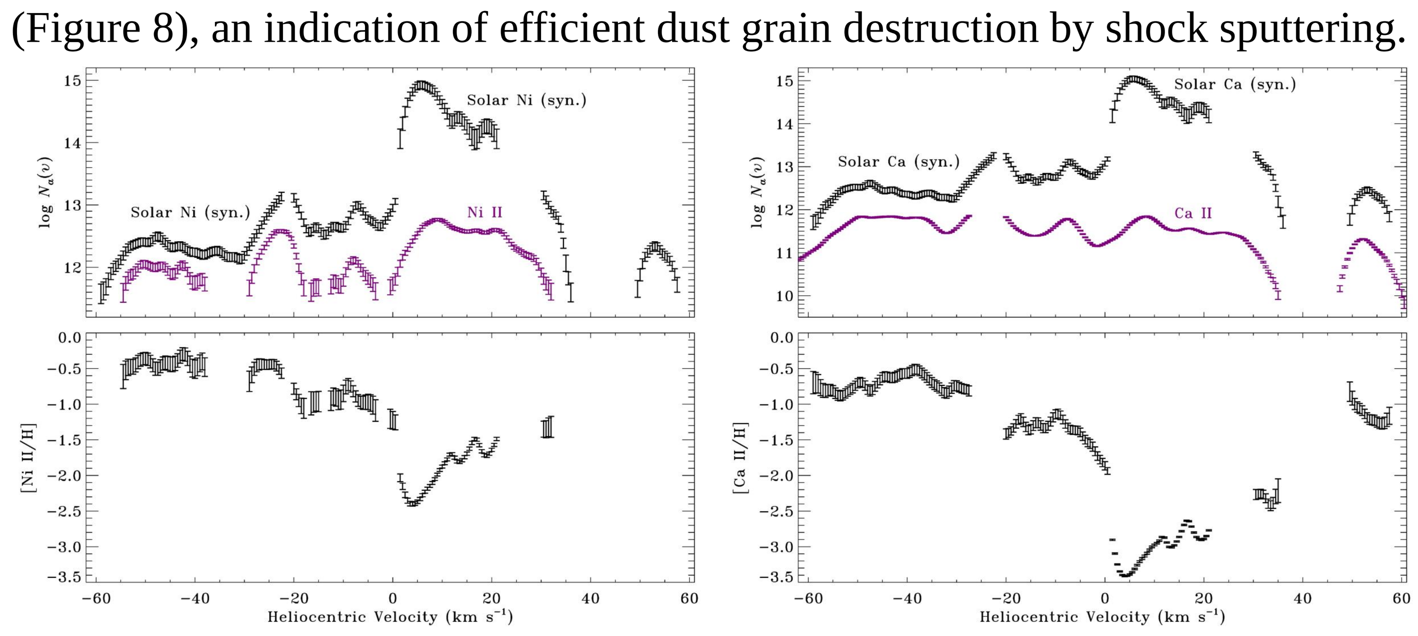

Figure 8: Upper panels: Apparent column density profiles of Ni II (left) and Ca II (right) toward HD 43582. The "solar" Ni and Ca profiles indicate the total (gas + dust) abundances as a function of velocity. These are constructed from a combination of the O I λ1355 line at the highest column densities and the S II λ1250 and λ1259 lines at lower column densities. Lower panels: The corresponding Ni II and Ca II depletion factors.

Asaoka, I., & Aschenbach, B. 1994, A&A, 284, 573
Gaensler, B. M., Chatterjee, S., Slane, P. O., et al. 2006, ApJ, 648, 1037
Jenkins, E. B., & Tripp, T. M. 2001, ApJS, 137, 297
Jenkins, E. B., & Tripp, T. M. 2011, ApJ, 734, 65
Taylor, C. J., Ritchey, A. M., Federman, S. R., & Lambert, D. L. 2012, ApJL, 750, L15

Support for this work was provided by NASA through grant HST-GO-13709.001-A from the Space Telescope Science Institute.